JOURNAL OF SPACECRAFT AND ROCKETS
Vol. 32, No. 1, January–February 1995

Minimum-Mass Design of Sandwich Aerobrakes for a Lunar Transfer Vehicle

K. N. Shivakumar* and J. C. Riddick†
North Carolina A&T State University, Greensboro, North Carolina 27411

A structural mass optimization study of a sandwich aerobrake for a lunar transfer vehicle was conducted. The proposed spherical aerobrake had a base diameter of 15.2 m and radius of 13.6 m. A hot thermal protection system (TPS) and cold structure were used in the design. Honeycomb sandwich aerobrake structures made up of four different materials—aluminum alloy, titanium alloy, graphite-epoxy, and graphite-polyimide—were considered. Cases of aerodynamic load, equivalent uniform pressure, and aerodynamic plus thermal load were analyzed. Both linear stress and buckling analyses were conducted for a range of skin and core thicknesses. A graphical optimization procedure was used to determine the skin and core thicknesses of a minimum-mass aerobrake. The design criteria used were material strength, global buckling, and TPS tile deformation. Among them, the TPS deformation criterion was the most critical. The graphite-epoxy aerobrake was the lightest among the four materials studied. Its total mass is about 12.3% of the LTV mass, for supports at 75% span. Equivalent uniform loading produced smaller deformations, stresses, and buckling loads than did the more realistic aerodynamic loading for the same aerobrake configuration. Thermally induced stresses countered the aerodynamically induced stresses and hence had a beneficial effect on the deformation and buckling of the aerobrake.

Nomenclature

m	= mass per unit area of the aerobrake wall, lb/in.^{2}
p	= aerodynamic pressure at any point on the convex surface of the aerobrake, lb/in.^{2}
p_0	= stagnation pressure, lb/in.^{2}
R_s	= radial distance of the payload support from the axis of the aerobrake, in.
r_x, r_y, r_z	= rotations about Cartesian axes x, y, z, respectively, deg
t_{core}	= aerobrake core thickness, in.
t_{skin}	= aerobrake skin thickness, in.
u, v, w	= displacements in Cartesian directions x, y, z, respectively, in.
ϕ	= spherical angle between the stagnation point and a point of interest on the surface on the aerobrake, deg
ρ_{core}	= density of the core material, lb/in.^{3}
ρ_{skin}	= density of the skin material, lb/in.^{3}

Introduction

ESTABLISHMENT of a lunar colony is considered a precursor mission to a human mission to Mars in the Space Exploration Initiative Program.[1] The transportation of materials and personnel from Earth to the moon is a major technical challenge because of the exorbitant cost of delivering payloads to Earth orbit and beyond. One method of reducing the overall transportation cost is through the use of a space-based reusable space transfer vehicle. In a lunar mission, the space-based lunar transfer vehicle (LTV) could reside at the space station Freedom and transfer payloads between the station and the moon.

The LTVs or similar transfer vehicles experience large velocity changes between interplanetary transfer orbit and Earth parking orbit (see Fig. 1). These types of maneuvers are referred to as capture. The two capture techniques currently being explored are propulsive and aerobraking. In a propulsive capture, a propellant required for a round trip to the Moon and return must be carried, which adds to the weight of the LTV. In the aerobraking capture, the velocity of the LTV is reduced by the aerodynamic drag created when the spacecraft enters the Earth's atmosphere (see Fig. 1). The aerobrake is reusable, and it may reduce the ground launch cost for multiple-mission scenarios. Generally an aerobrake is considered advantageous only if the aerobrake mass is less than the required propellant and propulsion-system mass. The general design guidelines dictate that the aerobraked LTV is advantageous only if the mass of the aerobrake is less than 15% of the mass of the transfer vehicle.[2] A study[3] has shown that for a 15-ton lunar payload, the aerobrake will save about 26% of the LTV gross mass in comparison with the propulsive LTV. This translates to a saving of almost one Earth-to-orbit flight for each orbit-Moon-return mission.

The analysis and design of aerobrakes form a multidisciplinary study involving aerodynamics, heat transfer, and structural analyses (see Fig. 2), as well as packaging and transportation. Aerodynamic and heat-transfer analyses are required for calculating aerodynamic drag pressure and thermal loads; the structural analysis is conducted to design the aerobrake to withstand aerothermal loads. The present study focuses on the structural design of the lunar aerobrake, with a minimum-weight structure as the primary goal. Two concepts are used in designing aerobrakes: a hot-cold structure and a hot structure. In the hot-cold concept, the aerobrake consists of two layers: the outer hot layer providing thermal barrier is the thermal protection system (TPS), and the inner cold layer is the load-bearing structure. In the hot-structure concept, the aerobrake is made up of a single monolithic material that will withstand both high temperatures and aerothermal loads. The hot-cold concept is used in the present study because of the availability of well-characterized lightweight materials for cold or nearly cold structures.

A number of aerobrake wall construction concepts have been studied in the literature for both lunar transfer and Mars transfer vehicles. The types of constructions studied were truss-panel,[4–7] stringer-panel,[8,9] and honeycomb stiffeners.[10,11] In many of the studies reported an equivalent uniform load was used instead of the nonuniform aerodynamic load. Objectives of this study are to conduct a mass optimization of a honeycomb-sandwich LTV aerobrake made of various aerospace structural materials and quantify the effect of payload support location, loading type (aerodynamic versus uniform pressure), and thermal gradient on the design parameters.

Honeycomb-sandwich aerobrake construction was selected for the minimum-weight design study because the honeycomb walls

Received June 3, 1993; revision received April 25, 1994; accepted for publication May 13, 1994.

*Research Professor, Department of Mechanical Engineering, Mars Mission Research Center. Associate Fellow AIAA.

†Graduate Student, Department of Mechanical Engineering, Mars Mission Research Center.

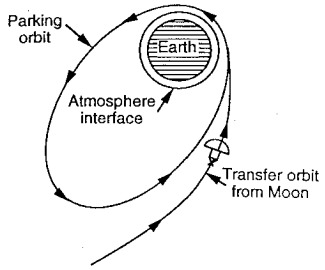

Fig. 1 Return of lunar transfer vehicle to Earth parking orbit.

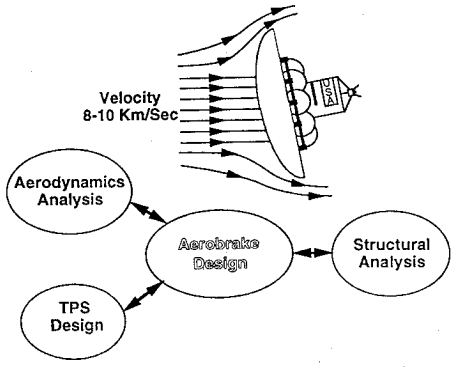

Fig. 2 Multidisciplinary analysis for design of an aerobrake.

are stiff and lightweight, and the usual moisture problems are not encountered in space applications. Several skin materials commonly used in the spacecraft industry are evaluated. Design details and the mass of the rigid TPS tile were taken from Ref. 12. Linear stress and buckling analyses of the aerobrake structure are conducted to establish the shell wall. A factor of safety of 1.4 is used to establish the allowable limits for material strength, buckling load, and TPS tile deformation criteria. Optimized skin and core thicknesses for aluminum, titanium, and polymeric composite (graphite-epoxy and graphite-polyimide) honeycomb-sandwich walls are calculated, and their masses are estimated and compared with each other.

Aerobrake Configuration and Loading

Figure 3 shows a spheroidal aerobrake configuration proposed by NASA Langley Research Center[12] for the LTV, based on the NASA Marshall Space Flight Center single-payload module of 25 feet (7.6 m) diameter. The spheroid base diameter is 50 ft (15.24 m), and the spheroid radius is 44.5 ft (13.5 m). Although aerobrakes will have an outer skirt to deflect the aerodynamic wake, this skirt is not considered in the structural analysis. Newtonian aerodynamic analysis was performed for a lunar transfer vehicle of mass 45,100 lb, entering the Earth atmosphere at an altitude of about 200,000 ft (61 km), angle of attack 11 deg, and a deceleration of $4.18g$. The analysis gave a stagnation pressure of 0.737 lb/in.^{2} (5.1 kPa). The aerodynamic pressure p at any other point on the surface of the aerobrake is approximated by the simple cosine-square formula as

$$p = p_0 \cos^2 \phi = 0.737 \cos^2 \phi \qquad (1)$$

The sectional view of the aerobrake configuration and the loading is shown in Fig. 3. The aerobrake and the payload module are assumed to be connected by eight equally spaced supports (see the plane view of the aerobrake in Fig. 4a). Two support locations are considered at 75% span (R_s = 18.75 ft = 5.7 m) and 50% span (R_s = 12.5 ft = 3.8 m). Membrane analysis of the aerobrake shell subjected to a uniform load showed that the hoop stress is reduced by 45% by moving the support location from the midspan to the 75%-span location. Similar results were reported in other aerobrake studies[5,6,9] with different concepts as well. Accordingly, the 75%-span location was chosen as the baseline study in this work.

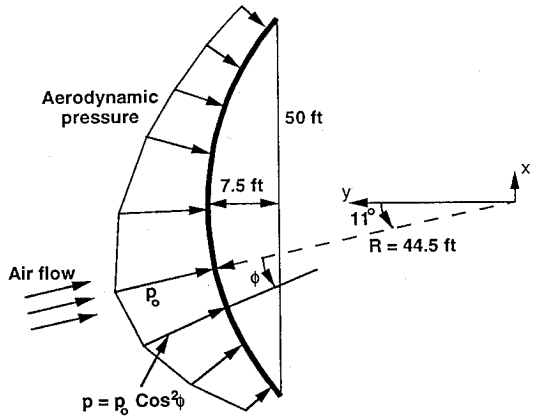

Fig. 3 LTV aerobrake configuration and loading.

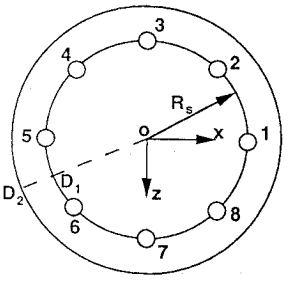

a) Eight-point support condition (not to scale)

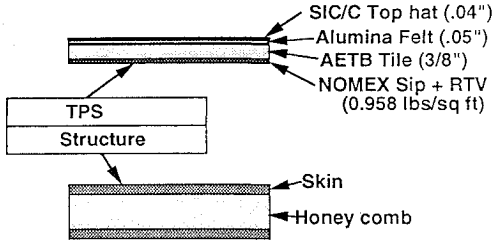

b) Aerobrake wall cross section

Fig. 4 Aerobrake supports and cross section.

Aerobrake Shell Wall Materials

Figure 4b shows the cross section of the hot-cold aerobrake wall. TPS tile data were taken from Ref. 12. The cold structure is a honeycomb sandwich shell with stiff inner and outer skins and a very light core material. Both skin and core thicknesses were assumed to be constant throughout the aerobrake shell. Four types of skin materials commonly used in aerospace structures are included in the study: high-strength aluminum alloy (7076 Al-T6), titanium alloy, graphite-epoxy composite (AS4-3501-6, quasi-isotropic lay-up), and graphite-polyimide (quasi-isotropic lay-up). The equivalent in-plane moduli, Poisson's ratios, ultimate strength, density, and maximum operating temperatures of these materials are given in Table 1. The core functions as a separator between the top and bottom skins. The modulus of elasticity of the core was assumed to be about 1% of the skin material, and the core density was about 0.002315 lb/in.^{3} (64 kg/m^3).

Design Constraints

The structural design of the aerobrake must satisfy the following three criteria:

1) The maximum effective (von Mises) stress is limited to 71% of the ultimate strength of the material.

2) The minimum buckling load factor is greater than or equal to 1.4.

3) The maximum local deformation is less than the TPS tile tipoff deformation.

Table 1 Material properties

Material	Modulus, Msi	Poisson's ratio	Ultimate strength, ksi	Density, lb/in.^{3}	Maximum temperature, °F
Aluminum	10.3	0.33	76.0	0.101	350
Titanium	16.4	0.31	130.0	0.160	750
Graphite-epoxy	14.4	0.32	44.0	0.063	260
Graphite-polyimide	8.2	0.34	76.0	0.057	500

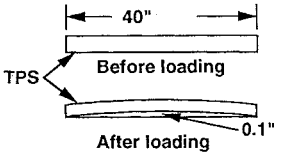

Fig. 5 TPS deformation criterion.

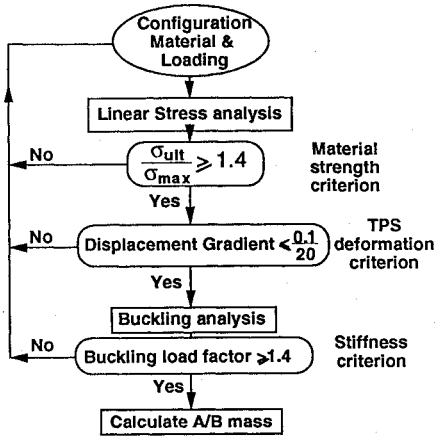

Fig. 6 Sizing flow chart of the LTV aerobrake.

The TPS tile deformation criterion needs more explanation. Figure 5 shows the TPS configuration before and after loading. The transverse deformation of the TPS at the midspan must be less than 0.1-in. (2.5 mm) over a 40-in. (1.0-m) span. This criterion can be treated as a change in either the radius of curvature or the gradient of the deformation. For simplicity, the gradient definition, that is, 0.1-in. (2.5-mm) deformation over a length of 20 in. (0.5 m), was used. Although other design parameters, such as joining, packaging, and transportation, are important, they are not considered in this paper. The flow diagram in Fig. 6 shows the various types of analyses and the design constraints used in the aerobrake sizing procedure.

Analysis of the Aerobrake Model

Linear stress and buckling analyses of the aerobrake were conducted using a commercial finite-element structural analysis code, ANSYS.[13] In the optimization procedure, the skin and the core thickness were used as variable parameters, and minimum mass as the objective function. A graphical optimization procedure was used to calculate the skin and core thicknesses of the aerobrake. The analysis was conducted for a series of skin and core thicknesses of an aluminum-skin and aluminum-honeycomb aerobrake. The skin thickness was varied from 0.01 in. (0.25 mm) to 0.05 in. (1.25 mm) in steps of 0.01 in. (0.25 mm), and the core thickness was varied from 1.0 in. (25 mm) to 5.0 in. (125 mm) in steps of 1.0 in. (25 mm). The maximum effective stress (outside the support point), deflection at critical sections, and buckling loads were calculated. The graphical procedure was used to establish the optimum skin and core thicknesses. The thicknesses for graphite-epoxy, graphite-polyimide, and titanium sandwich shells were also calculated from the normalized graphs generated for aluminum and then checked via the reanalysis. The normalization was based on the aluminum-model elastic modulus.

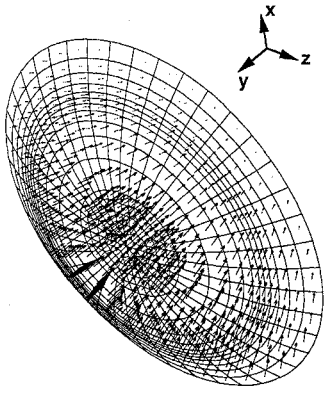

Fig. 7 Aerobrake model and aerodynamic loading.

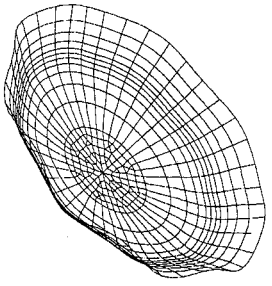

Fig. 8 Deformed shape of the LTV aerobrake.

Finite-Element Model

Figure 7 shows the finite-element idealization and the aerodynamic loading of the spherical aerobrake. The length of the arrows represents the magnitude of the pressure. Eight-node isoparametric layered shell elements were used in the finite-element idealization. The degrees of freedom at each node were three displacements u, v, and w in the Cartesian directions x, y, and z, respectively, and three rotations r_x, r_y, and r_z about the three Cartesian axes. The model had 584 elements and 1769 nodes with 10,614 degrees of freedom. The structural configuration and the loading are symmetric about the x-y plane. Hence one half of the symmetrical model was used in the analysis; for the purpose of illustration the complete shell is shown in Fig. 7. The aerodynamic loading on the convex portion of the aerobrake is shown by the pressure vectors in Fig. 7. The eight supports are located 45 deg apart, as shown in Fig. 4a, at a radius 18.75 ft (5.7 m) from the axis of the shell. All three displacements, u, v, and w, were set to zero at the eight supports to simulate a fully fixed payload attachment.

Linear Stress Analysis

A linear stress analysis of the aluminum aerobrake model was conducted for a range of skin and core thicknesses mentioned previously. Figure 8 shows a typical deformed shape of the aerobrake for skin and core thicknesses of 0.03 in. (0.75 mm) and 2.0 in. (50 mm), respectively. The maximum normal deflection occurred along the meridian 22.5 deg from the negative x axis. Nodal points D_1 and D_2 (see Fig. 4a) were selected to calculate the displacement gradient and then to verify the deformation criterion of the TPS tile. Figure 9 shows the effective stress contours at the outer surface of the aerobrake. As expected, there is a high stress concentration at the support locations. Since a stiff core material was used along the

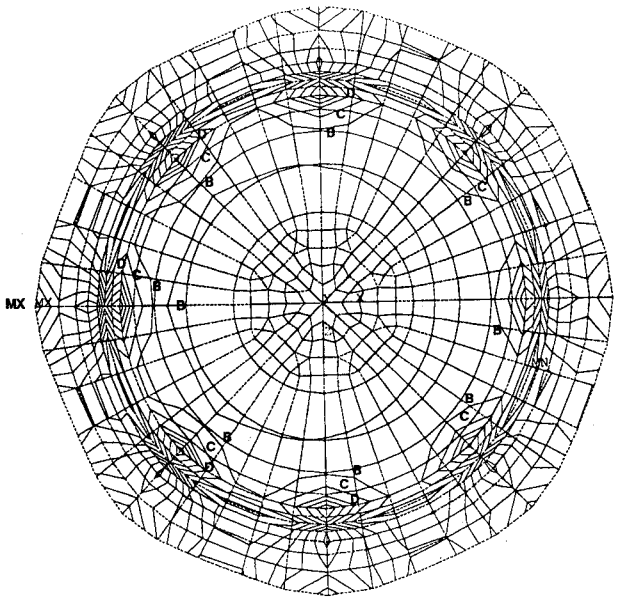

Fig. 9 Effective stress contour of the LTV aerobrake; B = 2.046 ksi, C = 2.873 ksi, D = 3.701 ksi, and MX = 8.251 ksi.

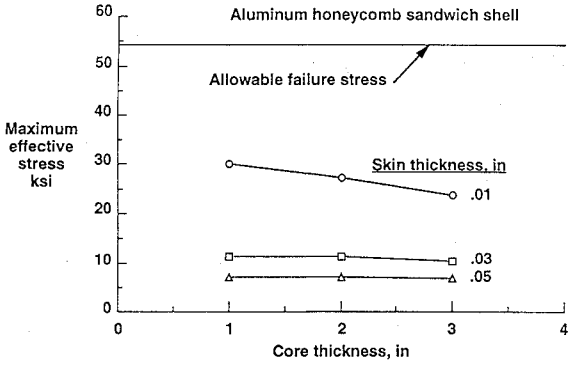

Fig. 10 Variation of the maximum effective stress with skin and core thicknesses of the aluminum aerobrake.

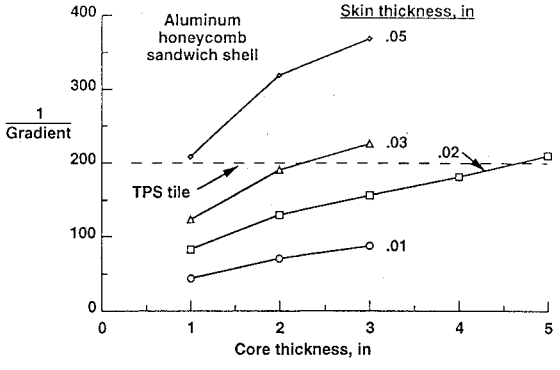

Fig. 11 Variation of displacement gradient with skin and core thickness of the aluminum aerobrake.

support ring, the maximum stress occurred at the location represented by MX in Fig. 9. Examination of the three principal stresses in the top and bottom skins of the aerobrake showed that all stresses were primarily compressive except near the support.

Figure 10 presents the variation of the maximum effective stress with skin and core thickness for the aluminum aerobrakes. The allowable stress, based on the factor of safety of 1.4, is shown by a dashed horizontal line. For the range of configurations analyzed, the maximum effective stress is far smaller than the allowable stress. The variation of the reciprocal of the displacement gradient with skin and core thicknesses is shown in Fig. 11. As mentioned previously,

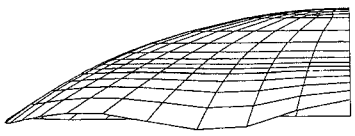

Fig. 12 First buckling mode of half of the symmetrical LTV aerobrake.

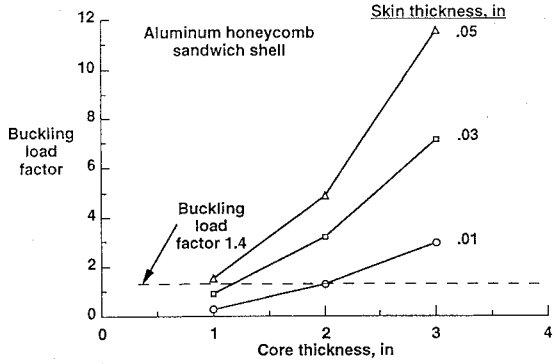

Fig. 13 Variation of the buckling load factor with skin and core thicknesses for the aluminum aerobrake.

the gradient was calculated from the displacements at D_1 and D_2 (see Fig. 4a). The allowable gradient for the TPS tile is $\frac{1}{200}$ and is shown by the horizontal line. All configurations above this line satisfy the TPS tile deformation criterion. Comparison of Figs. 10 and 11 shows that the TPS tile deformation criterion is a more critical design parameter than the maximum-local-stress criterion.

Buckling Analysis

The buckling analysis of the aerobrake was performed after the linear stress analysis, using the calculated stress field as the initial stress. A typical first mode of buckling of the aerobrake model is shown in Fig. 12. The buckling mode shape is symmetric about the x axis (because of the symmetry of the configuration and loading); hence only one half of the model is shown. The first buckling mode for other skin and core thicknesses and materials was similar to that shown in Fig. 12. A variation of the buckling load factor for $p_0 = 0.737$ lb/in.^{2} (5.1 kPa) with the aerobrake skin and core thicknesses is shown in Fig. 13. The buckling load factor varied nearly linearly with the skin thickness and quadratically with the core thickness. A wide range of skin and core thicknesses result in a buckling load factor more than 1.4. Results in Figs. 10, 11, and 13 show, repeatedly, that the TPS tile deformation is the most critical criterion in the design of an aerobrake.

Minimum-Mass Aerobrake Configurations

Parametric results of the previous sections and the mass equation were used to establish the minimum-mass aerobrake. As concluded previously, the TPS tile deformation criterion dictated the aerobrake wall configuration. All possible skin and core thicknesses that satisfy the TPS tile deformation criteria were extracted from Figs. 10, 11, and 13 and are summarized in Fig. 14 for the aluminum aerobrake. The dashed lines are the mass density (mass per unit surface area) of the aerobrake. The aerobrake mass density m is calculated from the equation

$$m = 2t_{\text{skin}}\rho_{\text{skin}} + t_{\text{core}}\rho_{\text{core}} \tag{2}$$

The core density ρ_{core} is 0.002315 lb/in.^{3} (64 kg/m^3) and was assumed the same for all sandwich constructions. The densities of the skin materials are given in Table 1. The solid line joining the triangle symbols in Fig. 14 is the buckling critical curve. All configurations above this line have the buckling factor of safety greater than 1.4. The buckling optimum configuration had skin and core thicknesses of 0.0012 in. (0.03 mm) and 2.5 in. (62.5 mm), respectively. The solid line joining the circle symbols is the TPS tile deformation critical curve. All configurations above this line satisfy all three design criteria. Because the material-strength critical curve lies outside the

Table 2 Aerobrake mass for four different material systems for supports at 75% span

Material	Thickness, in.		Density m, lb/in.^{2}	Aerobrake mass, lb		Fraction of LTV mass,%
	Skin	Core		Structure	Total	
Aluminum	0.030	2.0	0.01069	3308	6417	14.2
Titanium	0.015	3.0	0.01175	3635	6842	15.2
Graphite-epoxy	0.040	1.5	0.00852	2636	5543	12.3
Graphite-polyimide	0.045	3.8	0.00973	3011	6031	13.4

Table 3 Aerobrake mass for four different material systems for supports at 50% span

Material	Thickness, in.		Density m, lb/in.^{2}	Aerobrake mass, lb		Fraction of LTV mass,%
	Skin	Core		Structure	Total	
Aluminum	0.020	3.55	0.01226	3781	6974	15.5
Titanium	0.015	3.25	0.01232	3814	7018	15.6
Graphite-epoxy	0.045	2.00	0.01030	3188	6203	13.8
Graphite-polyimide	0.045	3.65	0.01126	3487	6592	14.6

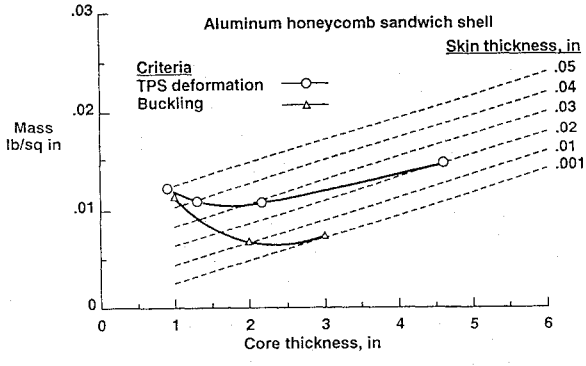

Fig. 14 Variation of the mass of the aluminum aerobrake with skin and core thicknesses.

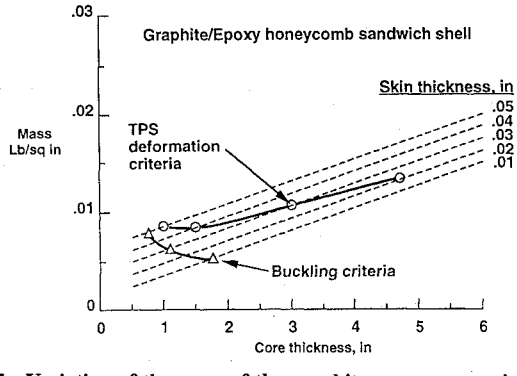

Fig. 15 Variation of the mass of the graphite-epoxy composite aerobrake with skin and core thicknesses.

range of the graph, it is ignored. The configuration that had the lowest mass and satisfied the TPS deformation criterion had skin thickness 0.03 in. (0.75 mm) and core thicknesses 2.0 in. (50 mm). The calculated factors of safety based on the material strength and the buckling load were 9.2 and 3.5, respectively.

Figure 15 presents the buckling critical and TPS deformation critical curves for the graphite/epoxy skin aerobrake. Notice again that the TPS deformation dictates the minimum mass of the aerobrake. Conversely, a more flexible TPS tile could substantially reduce the mass of the aerobrake.

Optimum skin and core thicknesses and the mass density for the four candidate materials are given in the Table 2. The total mass of the aerobrake was calculated from the product of the aerobrake surface area (309,466 in.^{2}, or 200 m^2) and the mass density of the aerobrake. Resulting masses of the aerobrake with and without the mass of joints are listed in Table 2. A linear slicing type of joining, which is considered[12] to be most efficient, was assumed. This joint mass was assumed to be about 30% of the structural mass. The total-mass column includes the TPS mass[12] (0.985 lb/ft^2). Among the four materials considered, the graphite/epoxy sandwich aerobrake is the lightest, with a mass of 5543 lb (2514 kg), or 12.3% of the proposed LTV mass (45,100 lb, or 20,315 kg). The values in the last column are the ratio of the aerobrake mass to the LTV mass.

The aerobrake wall configurations and the masses, given in Table 3 are for the supports located at 50% span (R_s = 150 in., or 3.8 m). Again note that the graphite-epoxy sandwich aerobrake had the lowest mass among the four materials considered. The total mass of the aerobrake, including the joints and the TPS, is 6203 lb (2843 kg), or 13.8% of the LTV mass. This configuration is about 12% heavier than the aerobrake with supports located at 75% span.

Analysis of Uniformly Loaded Aerobrake

In many past design studies, the aerodynamic loading was replaced by an equivalent uniform load, so that the problem reduced to an axisymmetric case, because the axisymmetric problem is much simpler than the complete shell analysis. The effect of such a simplification on the deformation, stress field, and buckling load is investigated here. Linear stress and buckling analyses of the optimized aluminum aerobrake configuration, t_{skin} = 0.03 in. (0.75 mm) and t_{core} = 2.0 in. (50 mm) were conducted by imposing the equivalent uniform pressure. The equivalent uniform pressure was calculated by matching the resultant y-directional force from the aerodynamic and uniform pressure loads. The equivalent uniform pressure was found to be 0.6 lb/in.^{2} (4.14 kPa). This uniform pressure was imposed on the finite-element model shown in Fig. 7, and the analyses were conducted. The payload supports were assumed to be at 75% span. Figure 16 shows the variation of v displacement along the meridian at an angle of 202.5 deg from the x axis (along the line OD_1D_2 in the Fig. 4a). Note that the displacements for uniform pressure are less than those for aerodynamic pressure. The maximum difference of about 15% occurs at the apex of the aerobrake.

The uniform pressure produced the maximum effective stress of 7462 lb/in.^{2} (51.5 MPa), which is about 9.6% lower than that for the aerodynamic pressure [8,251 lb/in.^{2} (56.9 MPa)]. The buckling load for uniform pressure is 2.20 lb/in.^{2} (the buckling load factor is 3.66), which is about 14% less than that for the aerodynamic pressure (2.62 lb/in.^{2}; the buckling load factor is 3.55 and the applied pressure is 0.737 psi). The equivalent-uniform-pressure approximation of the aerodynamic load produces lower deflection, stresses, and buckling loads; hence appropriate corrections should be made in the design of aerobrakes.

Table 4 Effect of thermal loads on the design parameters

Parameter	Aluminum shell		Graphite-epoxy shell	
	Aerodynamic load	Aerothermal load	Aerodynamic load	Aerothermal load
Maximum effective stress, ksi	8.23	38.54	9.35	34.26
Buckling load factor	3.89	3.46	3.46	5.31
Maximum displacement gradient	−1/350	1/1360	−1/420	1/1280

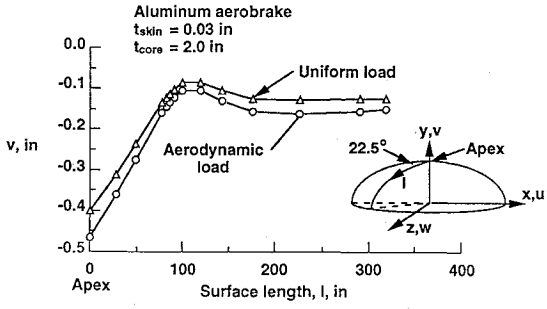

Fig. 16 Variation of the v displacement along the meridian at 202.5 deg from the x axis.

Effect of Thermal Loads

Aerothermal analysis of the LTV aerobrake reported in Ref. 12 showed that the backface temperature of the TPS ranges from 220 to 260°F, depending on the heat-conduction properties of the structural materials. Note that all material properties were assumed to be constant in the temperature range considered. For the purpose of qualitative investigation of the effect of thermal loading on the design parameters of the aerobrake, a temperature distribution varying linearly from 240°F at the outer surface of the outer skin to 70°F at the inner surface of the inner skin was assumed. Thermal expansion coefficients for aluminum and the quasi-isotropic graphite-epoxy (from the handbooks) are 12.4×10^{-6} and 8.6×10^{-6}°F^{-1}, respectively. Aerothermal (aerodynamic load + thermal load) stress and buckling analyses of optimized configurations of aluminum and graphite-epoxy composite aerobrakes were conducted. The payload supports were assumed to be at 75% span of the aerobrake. Results showed that the thermal load counteracted the stresses caused by the aerodynamic loads. Calculated maximum effective stresses, buckling load factors, and displacement gradients are listed in Table 4 for aerodynamic load alone and for aerodynamic plus thermal loads. The thermal load caused a threefold increase in the effective stress and caused the displacement gradient to drop to a third. Note also the reversal in the sign of the displacement gradient. The thermal loads increased the buckling load factors by about 20 and 53% for aluminum and graphite-epoxy aerobrakes, respectively. Because the thermal stresses oppose the aerodynamic stresses, thermal loads will have a beneficial effect in reducing the deformation gradient and increasing buckling load factors. However, the thermal stresses need to be evaluated accurately to verify that the stresses do not exceed the strength of the material.

Concluding Remarks

A structural mass optimization study of a sandwich aerobrake for a LTV was conducted. The proposed spherical aerobrake had a base diameter of 50 ft (15.2 m) and a radius of 44.5 ft (13.6 m). A hot TPS and cold structure were used in the design. Honeycomb sandwich aerobrake structures made up of four different materials—aluminum alloy, titanium alloy, graphite-epoxy, and graphite-polyimide—were considered. Cases of aerodynamic load, equivalent uniform pressure, and aerodynamic plus thermal load were analyzed. Both linear stress and buckling analyses were conducted for a range of skin and core thicknesses. A graphical optimization procedure was used to determine the skin and core thicknesses of a minimum-mass aerobrake. The design criteria used were material strength, global buckling, and TPS tile deformation. Among them, the TPS tile deformation criterion was the most critical. The graphite-epoxy aerobrake was the lightest among the four materials studied. Its total mass is about 12.3% of the LTV mass, for supports at 75% span. Equivalent uniform loading produced smaller deformations, stresses, and buckling loads than did the more realistic aerodynamic loading for the same aerobrake configuration. Thermally induced stresses countered the aerodynamically induced stresses and hence had a beneficial effect on the deformation and buckling of the aerobrake. The design study presented is preliminary, and a number of other factors, such as transient dynamic and thermal responses and thickness tapering, were not considered.

Acknowledgments

The authors acknowledge the financial support of the Mars Mission Research Center, established by Grant NAGW-1331 from NASA, Washington, DC, and the computational support of the North Carolina Supercomputing Center, Research Triangle Park, North Carolina.

References

[1]Pioneering Space Center, *Report on the National Commission on Space*, Bantam Books, 1986.

[2]Rehder, J. J., Cruz, C. I., Braun, K. E., and Bush, L. B., "An Aerobrake Concept for Lunar Return," NASA TP-3262, Dec. 1992.

[3]Anon., "Lunar Aerobraking Vehicle Operations and Cost," Phase 2 Report, McDonnell Douglas Space Systems Co., April 1991.

[4]Dorsey, J. T., and Mikulas, M. M., Jr., "Preliminary Design of a Large Tetrahedral Truss/Hexagonal Heatshield Panel Aerobrake," NASA TM 101612, Sept. 1989.

[5]Washington, G., and Klang, E., "Modeling and Analysis of Doubly Curved Aerobrake Truss Structures," *Proceedings of the 3rd International Conference on Engineering, Construction, and Operations in Space*, SPACE '92, Denver, CO, May 1992.

[6]Raju, I. S., and Craft, W. J., "Analysis and Sizing of a Mars Aerobrake Structure," *Journal of Spacecraft and Rockets*, Vol. 30, No. 1, 1993, pp. 102–110.

[7]Dorsey, J., Watson, J., and Tutterow, R., "Structural Concepts for Lunar Transfer Vehicle Aerobrake Which Can Be Assembled on Orbit," AIAA Paper 93-1394, 1993.

[8]Woodcock, G., "Review of Boeing Studies of Pathfinder Missions Involving High Energy Aerobraking," presented at 3rd Pathfinder Technical Integration Panel Meeting, Marshall Space Fight Center, Huntsville, AL, May 1989.

[9]Hairr, J., and Klang, E., "Structural Considerations in the Design of a Mars Mission Aerobrake," *Proceedings of the 3rd International Conference on Engineering, Construction, and Operations in Space*, SPACE '92, Denver, CO, May 1992.

[10]Bush, L. B., and Unal, R., "Preliminary Structural Design of a Lunar Transfer Vehicle Aerobrake," AIAA Paper No. 92-1108, 1992.

[11]Shivakumar, K. N., Craft, W. J., and Riddick, J. C., "Mass Estimation of Lunar Aerobrake Models Made Up of Various Aerospace Materials," *AD-Vol. 31, Space Exploration Science and Technologies Research*, American Society of Mechanical Engineers, New York, 1992, pp. 83–94.

[12]Katzberg, S. J., Butler, D. H., Doggett, W. R., Russell, J. W., and Hurban, T., "Aerobrake Assembly with Minimum Space Station Accommodation," NASA TM-102778, Oct. 1990.

[13]DeSalvo, G. J., and Gorman, R. W., *ANSYS Engineering Analysis System User's Manual*, Version 4.4, Swanson Analysis Systems, Inc., Houston, PA, May 1989.